3-25-2024

Investigation of Rare Earth Element Binding to a Surface-Bound Affinity Peptide Derived from EF-Hand Loop I of Lanmodulin

Geeta Verma

Jacob D. Hostert

Alex A. Summerville

Christine E. Duval

Julie N. Renner

ACS APPLIED MATERIALS & INTERFACES

www.acsami.org
Research Article

Investigation of Rare Earth Element Binding to a Surface-Bound Affinity Peptide Derived from EF-Hand Loop I of Lanmodulin

Geeta Verma,[⊥] Jacob Hostert,[⊥] Alex A. Summerville, Alicia S. Robang, Ricardo Garcia Carcamo, Anant K. Paravastu, Rachel B. Getman, Christine E. Duval, and Julie Renner*

Cite This: ACS Appl. Mater. Interfaces 2024, 16, 16912−16926
Read Online

ACCESS | Metrics & More | Article Recommendations | Supporting Information

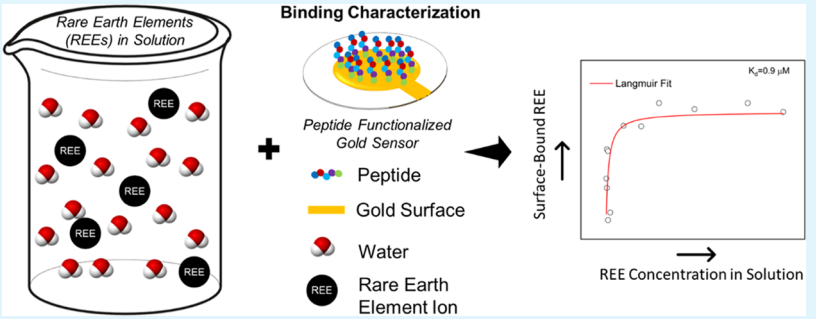

ABSTRACT: Bioinspired strategies have been given extensive attention for the recovery of rare earth elements (REEs) from waste streams because of their high selectivity, regeneration potential, and sustainability as well as low cost. Lanmodulin protein is an emerging biotechnology that is highly selective for REE binding. Mimicking lanmodulin with shorter peptides is advantageous because they are simpler and potentially easier to manipulate and optimize. Lanmodulin-derived peptides have been found to bind REEs, but their properties have not been explored when immobilized on solid substrates, which is required for many advanced separation technologies. Here, two peptides, LanM1 and scrambled LanM1, are designed from the EF-hand loop 1 of lanmodulin and investigated for their binding affinity toward different REEs when surface-bound. First, the ability of LanM1 to bind REEs was confirmed and characterized in solution using circular dichroism (CD), nuclear magnetic resonance (NMR), and molecular dynamics (MD) simulations for Ce(III) ions. Isothermal titration calorimetry (ITC) was used to further analyze the binding of the LanM1 to Ce(III), Nd(III), Eu(III), and Y(III) ions and in low-pH conditions. The performance of the immobilized peptides on a model gold surface was examined using a quartz crystal microbalance with dissipation (QCM-D). The studies show that the LanM1 peptide has a stronger REE binding affinity than that of scrambled LanM1 when in solution and when immobilized on a gold surface. QCM-D data were fit to the Langmuir adsorption model to estimate the surface-bound dissociation constant (K_d) of LanM1 with Ce(III) and Nd(III). The results indicate that LanM1 peptides maintain a high affinity for REEs when immobilized, and surface-bound LanM1 has no affinity for potential competitor calcium and copper ions. The utility of surface-bound LanM1 peptides was further demonstrated by immobilizing them to gold nanoparticles (GNPs) and capturing REEs from solution in experiments utilizing an Arsenazo III-based colorimetric dye displacement assay and ultraviolet−visible (UV−vis) spectrophotometry. The saturated adsorption capacity of GNPs was estimated to be around 3.5 μmol REE/g for Ce(III), Nd(III), Eu(III), and Y(III) ions, with no binding of non-REE Ca(II) ions observed.

KEYWORDS: *rare earth elements, biosorption, gold nanoparticles, affinity peptides, lanmodulin, molecular dynamics*

INTRODUCTION

Rare earth elements (REEs) are essential in several emerging technologies such as wind turbines, electric vehicles, computer memory, autocatalytic converters, magnetic resonance imaging, and smartphones.[1] Because REEs are valuable and have limited availability, the recovery of these elements from industrial waste streams is an attractive option for a green and circular economy.[2] There is an urgent need to identify efficient separation methods that recycle REEs from waste streams and provide a steady, domestic source of these elements. Various techniques have been applied to recover REEs from the waste streams such as solvent extraction,[3] filtration,[4] ion exchange,[5] chemical precipitation,[6] adsorption,[7] and electrochemical processes.[8] Commercially, solvent extraction is used to separate REEs from

Received: November 22, 2023
Revised: January 17, 2024
Accepted: February 27, 2024
Published: March 25, 2024

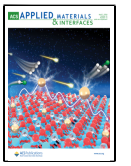

concentrated aqueous waste streams, but the solvent requirements are high in this method.[9] Membrane filtration techniques do well under low concentration and high volume throughput conditions, but the limiting factor is the selectivity of commercial membranes for trivalent ions over divalent ions.[10] Overall, some of the constraints of these methods include high chemical consumption, high operational cost, and the need to treat the generated waste.[11] To overcome these challenges, innovative developments utilizing several emerging technologies such as nanomaterials, bioleaching, biosorption, acidolysis, biomineralization, cryomilling, and the use of supercritical carbon dioxide[12] are under investigation. Among these, there are several advantages of biocombined (biosorption) recycling strategies as they show higher selectivity, use fewer toxic chemicals, have high regeneration potential, demonstrate fast kinetics, and are cost-efficient.[13] However, the design of a biobased approach with selective adsorption of REEs requires deep acquaintance with the support materials and the ligand of choice such as peptides that can be grafted on the desired surface for selective separation of REEs. Peptides are desirable as they are short chains of amino acids (less than 50) and are highly tunable ligands that are selective for ions.[14] Many researchers have attempted to identify or design peptides with the ability to selectively bind to lanthanides.[13,15,16] For example, Hatanaka et al.[15] studied a linear peptide lanthanide-binding tag (LBT3) and by combining experimental and computational techniques provided a deep insight into the mechanism underlying the specificity of the peptide toward lanthanides in aqueous media. Through isothermal titration calorimetry (ITC) experiments, they found that the thermodynamic properties of ion complexation strongly vary with lanthanide ion size, and molecular dynamics (MD) simulations revealed that the high binding affinity is achieved through complete ion dehydration. In another investigation, Xu et al.[16] derived a peptide sequence from the EF-hand loop I of calmodulin and experimentally showed that the peptide has the same affinity for cerium(III) ions when tethered to a gold surface (surface-bound) as it does in solution (unbound).[16,17]

The recent discovery of the lanmodulin protein, which has high selectivity for REEs over non-REEs,[18] opens new possibilities for utilizing lanmodulin-derived peptides for REE recovery. Lanmodulin has four metal-binding EF-hand motifs that undergo a large conformational change in response to REE binding (from a largely disordered state to a more ordered state) and has higher affinity over calmodulin.[19] As a result, several lanmodulin ion complexation studies have been conducted to understand its structure as well as its REE binding affinity and selectivity.[19−24] In a recent investigation of the four EF-hand loop peptides derived from lanmodulin, Gutenthaler et al.[24] examined their affinity for two REEs (Eu(III), Tb(III)) and one non-REE (Ca(II)) in solution and used molecular dynamics simulations to further support their experimental observations. While studies of the shorter peptides are limited, more work has been done to tether the full-length lanmodulin protein to various supports to perform separation. Kwon and co-workers[21] used elastin-like polypeptide (ELP) fused with truncated lanmodulin protein to form REE-sensitive and thermoresponsive genetically encoded ELP, called "RELP". They studied several REEs (Tb(III), La(III), Ce(III), and Y(III)) and non-REEs (Zn(II) and Cu(II)) in the bulk with the help of calorimetric techniques. Among limited solid surface-bound studies, Dong et al. immobilized lanmodulin protein on agarose microbeads through thiol-maleimide click chemistry and investigated the selectivity between REE pairs (Nd(III)/Dy(III) and Y(III)/Nd(III)) and grouped separation between heavy REEs Tb(III)−Lu(III) + Y(III) over light REEs (La(III)−Gd(III)) on a resin-packed column.[22] Ye et al.[23] immobilized lanmodulin protein on the surface of magnetic nanoparticles (MNPs) through SpyTag-SpyCatcher (Spy) chemistry and studied the binding of several REEs and non-REEs. Xie et al. engineered a bioadsorbent in which lanmodulin was displayed on the cell surface of the fungus *Yarrowia lipolytica* and the binding capacity for different REEs and non-REEs was characterized.[20] Although there are a few studies done on surface-bound lanmodulin protein, no such investigation has been done on lanmodulin-derived peptides for REE binding.

In this work, two novel peptides, LanM1 and scrambled LanM1, are derived from the EF-hand loop 1 of lanmodulin and are investigated against four REEs (Ce(III), Nd(III), Eu(III), and Y(III)) and two competing non-REEs (Ca(II) and Cu(II)) under surface-bound and unbound conditions. Cerium is selected as it is an important material in a wide range of applications such as oxygen sensing, industrial catalysis, fuel cells, low-temperature water−gas shift reactions, and electrochromic thin-film application.[25,26] Neodymium is used mainly in magnets, catalysts, and lasers.[27] Europium has applications in control rods for nuclear reactors, fluorescent bulbs, and optoelectronics.[1,28] Common uses of yttrium is in lasers, fluorescent lamps, and lighting.[27,29] We performed circular dichroism (CD) analysis and nuclear magnetic resonance (NMR) to confirm that the LanM1 peptide sequence modified for surface immobilization binds REEs. Isothermal calorimetry (ITC) experiments were performed to determine the thermodynamic parameters (K_D, ΔH, ΔS, and ΔG) of the interaction between the peptides and ions in solutions. QCM-D was conducted to show that surface-bound peptides derived from lanmodulin can bind REEs and to characterize the surface-bound affinity using the Langmuir adsorption model to estimate equilibrium binding constants. Molecular dynamics simulations were performed to gain molecular insights and to complement the experimental results. Finally, to demonstrate the utility of the surface-bound peptide as a material, the maximum REE adsorption capacity of LanM1 immobilized on gold nanoparticles was determined in a proof-of-concept experiment. Overall, this study characterizes the properties of surface-bound LanM1 peptide for the first time and demonstrates its potential utility in REE separation for further optimization and exploration in the future.

MATERIALS AND METHODS

Materials. The peptide sequences in this study were derived from the EF-hand loop I of lanmodulin and were ordered from GenScript (https://www.genscript.com/) at a purity of >95%. Cerium(III) chloride heptahydrate ($CeCl_3{\cdot}7H_2O$), 99.9% purity, neodymium nitrate hexahydrate ($Nd(NO_3)_3{\cdot}6H_2O$), 99.9% purity, europium(III) chloride hexahydrate ($EuCl_3{\cdot}6H_2O$), 99.9% purity, yttrium(III) chloride hexahydrate ($YCl_3{\cdot}6H_2O$), 99.9% purity, calcium sulfate dihydrate ($CaSO_2{\cdot}2H_2O$), 99.0% purity, and copper sulfate pentahydrate ($CuSO_2{\cdot}5H_2O$), 99.9% purity, were purchased from Sigma-Aldrich. Millipore ultrapure water (UPW) was used as a solvent. Nitrogen (N_2) gas (>99%) that was used in circular dichroism experiments was procured from Airgas. Gold nanoparticles with size less than 100 nm (powder), 99.9% trace, were obtained from Sigma-Aldrich.

Peptide Design. The peptide sequences for binding studies were designed from EF-hand loop I of lanmodulin. The sequence intended for REE binding is called LanM1 (Ac-CGGGDPDKDGTIDLKE-

https://doi.org/10.1021/acsami.3c17565
ACS Appl. Mater. Interfaces 2024, 16, 16912−16926

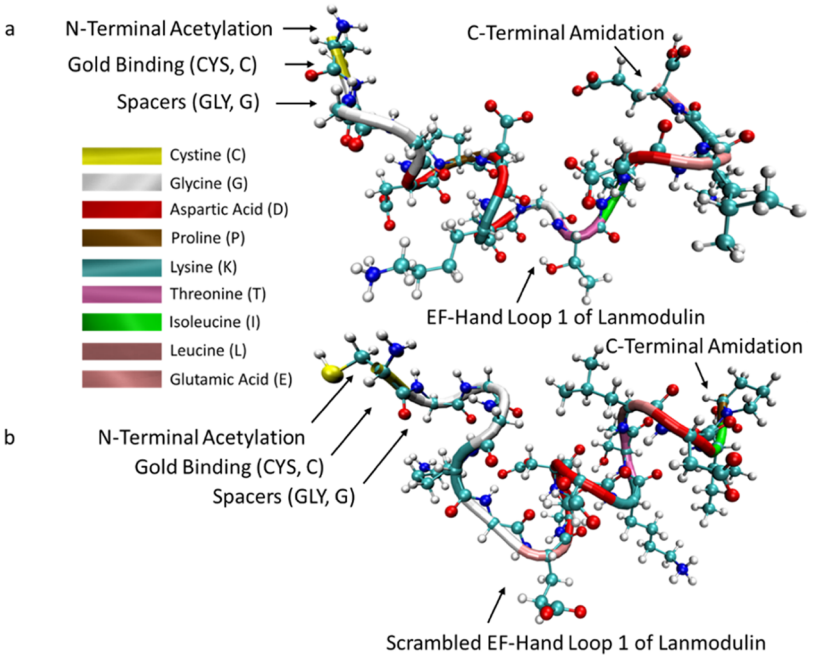

Figure 1. (a) Schematic representations of the energy-minimized peptide sequences LanM1 (Ac-CGGGDPDKDGTIDLKE-NH_2) and (b) scrambled LanM1 (Ac-CGGGKGEDDDKTLDIP-NH_2) designed in this study for cerium binding. Different colors in the backbone (tube representation) are used to show different amino acids in the sequence. The energy-minimized molecular images of the peptides were created using the visual molecular dynamics (VMD) package.[30]

NH_2). It is the same sequence as the EF hand loop I of lanmodulin with an additional three glycine amino acids as spacers and one cystine residue for binding to the gold surface. A schematic representation of LanM1 is given in Figure 1a. The second sequence, called scrambled LanM1 (Ac-CGGGKGEDDDKTLDIP-NH_2), has the same amino acids as in EF-hand loop I of lanmodulin, but they are randomly arranged with the same three glycine amino acids as spacers and one cystine for binding to the gold surface (Figure 1b). For both peptides, N-terminal acetylation and C-terminal amidation were done to increase the stability by reducing degradation.

Circular Dichroism (CD). A circular dichroism (CD) spectrometer (Jasco J-815) was used to examine the conformational change of the peptides under the influence of cerium(III) in ultrapure water. The step resolution of 0.1 nm and the scanning speed of 20 nm/min were selected to scan the samples in a quartz cuvette with 0.1 cm path length. The absorbance spectra were generated in the range of 190−260 nm wavelength. The postprocessing of the data including baseline correction and smoothing of the spectra was done using the Spectra Analysis processing tool of the Spectra Manager ver. 2.0 program, which accompanied the spectrometer.

^{1}H Nuclear Magnetic Resonance (NMR) Measurements. LanM1 and scrambled LanM1 samples were prepared by dissolving 1 mg of peptide in 0.75 mL of deuterated water (D_2O) and then pipetting them into 5 mm Wilmad NMR tubes. Each molar equivalent of cerium(III) was dissolved in 50 μL of D_2O before being added into NMR sample tubes. NMR measurements were collected on a 11.75 T magnet (500 MHz, ^{1}H NMR frequency) in a Bruker spectrometer. The Bruker default "zgesgp" pulse sequence for water suppression using excitation sculpting was used to collect the ^{1}H spectra. Signals were averaged over 100 scans.

Isothermal Titration Calorimetry (ITC). Isothermal titration calorimetry (ITC) analysis was performed by using a MicroCal Auto-ITC_{200}. In the present work, 200 μM REE solutions were titrated in 35 injections of 1 μL each with 300 μL of peptide solution (20 mM) at 30 °C. The solutions were prepared in ultrapure water, and prior to experiments, the solutions were degassed. The first injection point was removed due to the dilution/mixing effect and the baseline was corrected prior to further analysis. The data analysis was done with Origin 7.0 using the one set of site-fitting model to calculate the binding constant (K_d), enthalpy (ΔH), and entropy (ΔS). Adjustments to solution pH were made with HCl or NaOH as needed.

Quartz Crystal Microbalance (QCM). A quartz crystal microbalance with dissipation (QCM-D, Q-Sense Explorer, operated by Q-Soft integrated software from Biolin Scientific) was used to investigate the mass adsorption of the ions to surface-bound lanmodulin-derived peptides. Frequency shifts and dissipation changes were monitored simultaneously with time, and all experiments were conducted in an aqueous solution. Information about the gold-coated crystal sensors (QSX 301, 5 MHz, Biolin Scientific), module cleaning, and data analysis can be found in our previous work.[31] In general, QCM-D experiments were operated in a flow module at 18 °C and at a flow rate of 150 μL/min. The frequency decrease and increase reflect mass accumulation and removal on the surface, respectively, and dissipation changes show the viscoelastic characteristics of the adsorbed material. After acquiring a stable baseline with ultrapure water, lanmodulin peptides (Figure 1) were introduced at 10 μg/mL in ultrapure water and allowed to adsorb to the gold surface for 10 to 20 min before rinsing with ultrapure water to remove unbound peptides. Next, ion solutions were introduced to bind to the peptide for at least 10 min and then rinsed with ultrapure water to remove loosely bound ions. The QCM-D instrument is not sensitive enough to detect the REE loading on the peptide due to the extremely small added mass. To improve the sensitivity of detecting REE ion binding, a 1 mM sodium phosphate solution was then introduced for at least 10 min before a final rinse with ultrapure water. The exact mechanism of the phosphate interaction with REEs is still unclear. We speculate that coadsorbed water or precipitation along with the phosphate ions intensifies the frequency change.[17] This technique was validated with a known calmodulin peptide (Figure S7). The mass loading during the adsorption was estimated by using QSense Dfind software. The pH was ∼5.5 when analyzing the binding of REEs to surface-bound peptides.

MD Simulations. Molecular dynamics (MD) simulations were carried out using the GROMACS package.[32] First, the peptide sequences were drawn in ChimeraX,[33] and the coordinates were saved in the pdb format. The coordinate files in the pdb format were used to generate the topology and other input files using the GROMACS toolkit. By default, termini are ionized (NH_3^+ and COO^-); therefore, it is important to cap the N- and C-termini of the

https://doi.org/10.1021/acsami.3c17565
ACS Appl. Mater. Interfaces 2024, 16, 16912−16926

peptide to make them uncharged (NH_2 and COOH). Leaving the termini charged leads to artificial charge−charge interactions, particularly in small molecules like peptides. The CHARMM all-atom force field was selected to model peptides.[34] Cerium(III) was modeled as an LJ sphere with σ = 0.306 nm and ε = 0.0676 kcal/mol[35] with comparable parameters as other previously developed force fields.[36,37] Water molecules were represented with the TIP3P model as it is widely used for protein ligand simulation.[38] The geometric mixing rule was used to obtain the interaction parameters between unlike atoms. The initial configurations were generated by placing the peptides in the center of a cubic box with a side length of 5 nm. One cerium ion was inserted at some random position, and the boxes were solvated with explicit water molecules. The periodic boundary conditions were used in all directions. Prior to the simulation, the geometries of the systems were minimized using the steepest descent algorithm to remove any contact between the atoms. After geometry minimization, the systems were annealed from 600 to 300 K in an NVT ensemble for 5 ns. This was done to facilitate ion binding and overcome slow dynamics and any energy barrier and possible metastable stages. Finally, three independent 50 ns-long simulations were run in the NPT ensemble for the analysis. A time step of 2 fs was used with all bonds involving hydrogen atoms constrained by the LINCS algorithm.[39] The electrostatic interactions were treated using the fast particle-mesh Ewald (PME) summation method with a cutoff of 1.5 nm and a grid spacing of 0.1 nm.[40] The temperature was kept constant at 300 K using the velocity-rescale thermostat with a coupling constant of 0.1 ps.[41] In the NPT ensemble, 1 bar pressure was maintained used the Parrinello−Rahman pressure coupling with a coupling constant of 2.0 ps.[42] The trajectories obtained from the simulations were visualized in the VMD package, and coordination of oxygen atoms in the binding sites was monitored throughout the simulation.[30] A snapshot of the equilibrated configuration of the system composed of the peptide−ion complex after 50 ns is shown in Figure S1.

Adsorption Experiments on Gold Nanoparticles (GNPs). A protocol was prepared and used to estimate the adsorption of REEs on LanM1-functionalized GNPs. In all experiments, roughly 8 to 12 mg of GNP power was added to a 2.0 mL Eppendorf tube and the exact weight of GNPs was calculated by taking the weight of the tube before and after adding GNPs. Later, 1 mL of LanM1 solution at 60.2 μM concentration was added, and the tube was incubated on the rocker table for 24 h to saturate the GNPs with the peptide. Once LanM1 was functionalized on GNPs, the tube was centrifuged and the supernatant was removed. The LanM1-functionalized GNPs were then rinsed five times with ultrapure water to ensure no unbound LanM1 was left in the tube. The weight of the tube was measured again to estimate leftover water as it was not possible to pipette out all water after centrifugation and rinsing. In the following step, 1.5 mL of REE solution at a specific concentration between 20 and 125 μM was added to the tube and incubated again on a rocker table for another 24 h. During incubation, the concentration of GNP in the REE solution was 5−8 mg of GNP/mL. After centrifuging the tube, the supernatant was titrated against Arsenazo III reagent, and using the colorimetric technique, the concentration of the REE was estimated. Control experiments without GNP were performed to ensure that no metal leached from the tube material into the solution and no REE absorbed on the tube surface. A pictorial representation of the step-by-step procedure used for REE binding on gold nanoparticles (GNPs) is shown in Figure 8a. The initial and supernatant REE concentrations were used to determine the adsorption capacity of LanM1-functionalized GNPs. The pH of the solution remained between 5.0 and 5.5 throughout the experiment.

RESULTS AND DISCUSSION

Conformational Analysis and Binding Site Investigation. Both the peptides, LanM1 and scrambled LanM1, are newly designed peptides, and an initial binding investigation was needed to identify their ability to bind REE ions in solution. Therefore, the ability to bind to cerium(III) ions was checked using circular dichroism (CD) experiments, as we have done with other EF-hand peptide sequences previously.[16] Several experiments were performed by keeping the peptide concentration at 100 μM and varying the cerium(III) ion concentration within the range of 100 to 1000 μM. The effect of ion concentration on the secondary structure of the peptides was observed, and the spectra for LanM1 and scrambled LanM1 are reported in Figure 2a,b, respectively. In the case of LanM1, it was

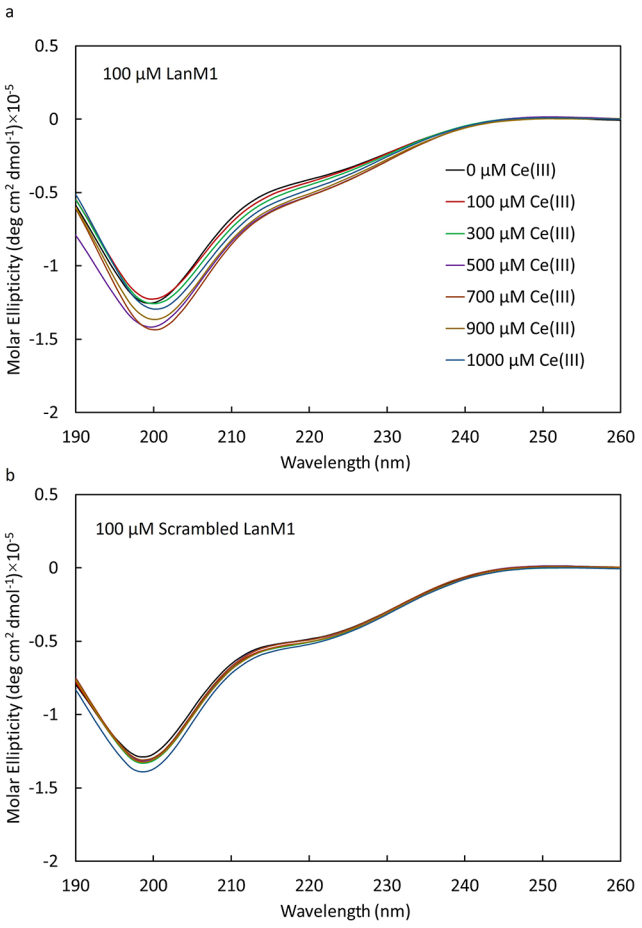

Figure 2. CD spectra of cerium(III) titration experiments with 100 μM (a) LanM1 peptide and (b) scrambled LanM1 peptide in DI water at different cerium(III) concentrations up to 1000 μM.

observed that at a wavelength of around 222 nm, there is a decrease in the ellipticity as the cerium ion concentration increases. It has been reported that decreases in the ellipticity at 222 nm are related to an increase in α-helicity caused by metal binding.[16,24] In the case of LanM1, a change in the structure of the peptide is confirmed upon REE binding with shifts at 200 and 222 nm observed. When looking at the spectra of scrambled LanM1, smaller changes in the ellipticity are observed, which indicate negligible shifts in the secondary structure of the peptide in the presence of cerium ions. A slight decrease in ellipticity at 200 nm was observed in the scrambled peptide at 1000 μM, which indicates an increase in the random coil content at high cerium ion concentrations. Although CD results could not quantify binding affinities of the designed peptides, the results indicate that the secondary structure of LanM1 undergoes larger structural changes upon binding than the scrambled peptide. To understand this change, molecular dynamics simulations were performed, and a conformational analysis of the peptides was carried out.

https://doi.org/10.1021/acsami.3c17565
ACS Appl. Mater. Interfaces 2024, 16, 16912−16926

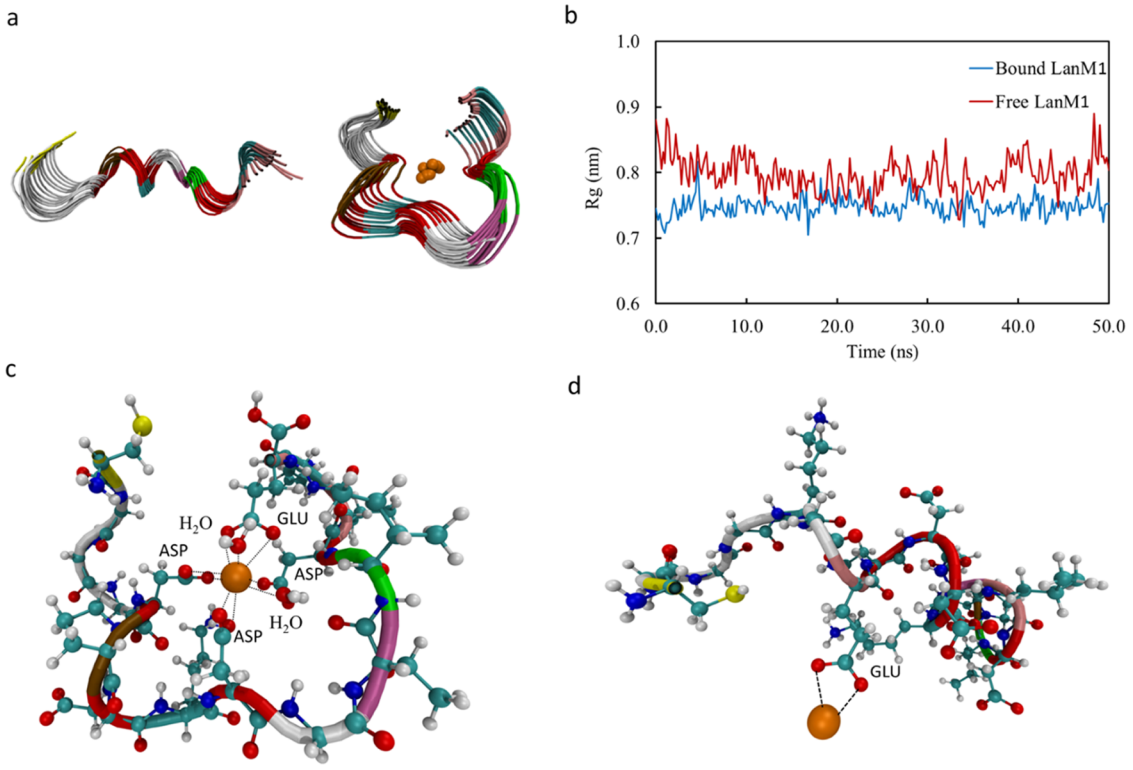

Figure 3. (a) Fifteen randomly selected superimposed MD snapshots of free LanM1 and cerium-bound LanM1 from the trajectory upon equilibration. Rod representation with different colors (same color scheme as in Figure 1) for amino acids is used for LanM1 and the cerium ion is presented in orange color. The water molecules are not displayed for clarity. (b) Radius of gyration (R_g) of the free (red) and ion-bound (blue) LanM1 in a 50 ns-long simulation. (c) Coordination of the cerium(III) ion with the LanM1 peptide after equilibration of the molecular dynamics simulation. A total of nine oxygen atoms are associated with the site. The cavity is formed with five oxygens from aspartic acid side chains, two from a glutamic acid side chain, and two water molecule oxygen atoms. (d) Cerium ion binding site in scrambled LanM1 peptide after equilibration. Only two oxygen atoms of glutamic acid are involved, resulting in weak binding and no "pocket" in comparison to LanM1.

Figure 3a shows randomly selected superimposed MD snapshots of free LanM1 and the LanM1−cerium(III) complex taken from 50 ns-long equilibrated trajectories. The visualization clearly indicates a well-preserved and equilibrated structure of LanM1 before and after binding with the ion. The snapshots illustrate a change in the conformation of the peptide upon binding that is consistent with the CD results. To better understand the change in the molecular conformation, the radii of gyration of the peptide in bound and free states are calculated and reported in Figure 3b. The results show that the radius of gyration of the free peptide is higher than that of the bound peptide. We suspect that this might be due to the peptide being more open in the free state and the structure becoming relatively rigid (packed) after complexation with the cerium ion. The other possible interpretation could be that the pocket presents more affinity toward the ion than with water; hence, the bound-state configuration is maximizing the ion−peptide interaction over the ion−solvent interaction. These findings are consistent with Gutenthaler et al., who had done a similar binding investigation of europium(III) ions with the EF-hand loops of lanmodulin.[24]

To gain atomistic details of the binding sites, Figure 3c shows the LanM1 binding site and the atoms that are coordinated with the Ce(III) ion. A total of nine oxygen atoms from LanM1 and water were observed to participate in the active binding site throughout the simulation. Out of these, seven were carboxylate oxygen atoms with five having an aspartic acid side chain and two having a glutamic acid side chain. The remaining two atoms were the oxygen atoms of water molecules near the binding site, as shown in Figure 3c. Cook et al. in their study determined the structure of all four metal-binding sites (EF-hand loops) of lanmodulin protein using NMR spectra when the binding sites were saturated with Y(III).[43] The atomistic investigation of the EF-hand loop I of lanmodulin bound to yttrium ions (the structure is available at the Protein Data Bank)[43] reveals that the binding site has nine oxygen atoms. However, in that case, no water molecules were associated in the binding site, defined as 2.3 Å distance from the ion. Gutenthaler et al. reported that the binding site for the Eu ion had a total of nine oxygen atoms with four atoms of aspartic acid and one of glutamic acid.[24] The remaining four oxygen atoms belong to the water molecules associated with the binding site. The number of water molecules coordinated in the inner sphere of lanthanide ions decreases from nine to eight across the series (La → Lu) due to the decreasing ionic radii. It has been found that the coordination number from La(III) to Nd(III) is nine; from Nd(III) to Tb(III), it is between nine and eight, and those from Tb(III) to Lu(III) have eight coordinated water molecules in the inner sphere.[44] In addition to the coordination number, the average ion−H_2O distance also varies with the atomic radii of REEs. For example, in the case of Sm(III), the average ion−H_2O distance is 2.474 Å and the value changes to 2.450 Å for Eu(III).[44] These factors together also impact the coordination chemistry of different ions when bound to the same binding site as found in different studies.[24,43,45] For example, in their study of lanthanide-dependent coordination interactions in lanmodulin, Liu et al. found that the coordination number of La(III) is 9.99

https://doi.org/10.1021/acsami.3c17565
ACS Appl. Mater. Interfaces 2024, 16, 16912−16926

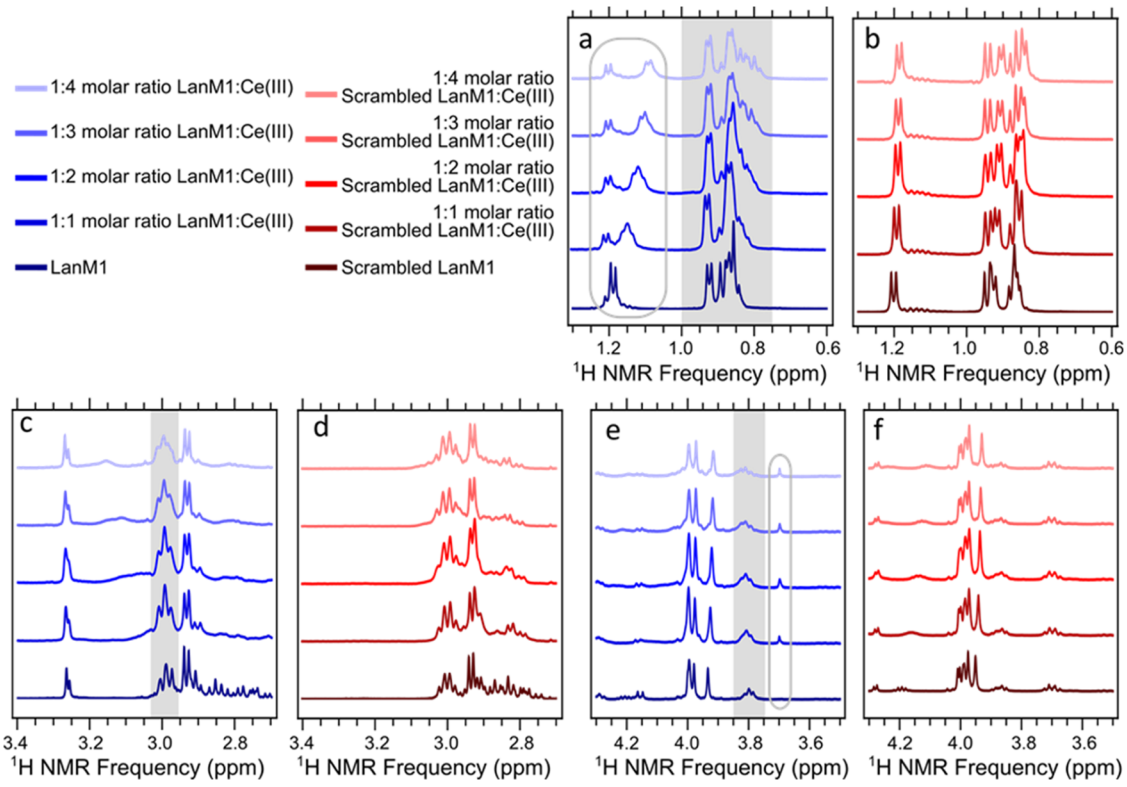

Figure 4. ^{1}H NMR measurements of the LanM1 peptide and scrambled LanM1 peptide at different molar ratios of peptide to cerium(III). (a, c, e) NMR spectra of LanM1 in blue (the shade gets lighter with increasing cerium(III) concentration from zero to 1:4 molar ratio). The NMR spectra for scrambled LanM1 are shown in red (the shade gets lighter with increasing cerium concentration from zero to 1:4 molar ratio) (b, d, f). Gray-highlighted regions in (a, c, e) identify peaks which experience line broadening as more cerium is added to the LanM1 peptide. Gray-encircled regions identify peak splitting or the emergence of new peaks.

with the EF-1 hand loop of lanmodulin, which changes to 9.00 in the case of Lu(III).[45]

When a similar analysis of the scrambled LanM1 (Figure 3d) was performed, no such multidentate binding was observed. Instead, a weak interaction was found with the two oxygen atoms of the glutamic acid, which is in good agreement with the observation made by CD spectroscopy. To further probe the LanM1 structure, an NMR study was conducted.

^{1}H solution NMR spectra of LanM1 and scrambled LanM1 at different NMR frequency ranges are shown side by side for comparison in Figure 4. We detect a greater effect on the spectra of LanM1 compared to scrambled LanM1 as cerium(III) is added to the peptide solutions. We suggest that the side chains within scrambled LanM1 may have transient interactions with the cerium(III) ions but not a cooperative binding effect that would result in distinct bound and unbound states. An additional control experiment conducted on polyproline, which does not bind to cerium(III), shows little to no change in ^{1}H NMR peaks and chemical shifts as cerium(III) is added (Figure S2).

As cerium(III) is added to LanM1, we observe broadening of peaks in the ranges of 0.75 to 1 ppm, 2.95 to 3.05, and 3.75 to 3.85 ppm (gray-highlighted regions in Figure 4a,c,e). We observe less broadening for the scrambled LanM1 sample as cerium(III) is added to the peptide solution (Figure 4b,d,f). ^{1}H NMR peaks in the 0.75 to 1 ppm range can be assigned to the leucine and isoleucine methyl groups. We also note peak splitting for LanM1 at 1.05 to 1.25 ppm in Figure 4a, which is within the ^{1}H NMR frequency range of the threonine methyl group.[46] Another difference in the NMR spectra is shown with the emergence of a new peak at ∼3.7 ppm in the LanM1 sample that does not appear in the scrambled LanM1 sample (Figure 4e,f). The line width of an NMR peak can be affected by the following factors when paramagnetic ions such as cerium(III) are involved: (1) distribution of conformations, (2) distance of the ^{1}H atom to the paramagnetic ion, and (3) dynamics, e.g., binding/unbinding of the ion, flipping between distinct conformations, and lifetimes of bound and unbound states.[47] When a ^{1}H atom is within spatial proximity, consistent with peptide binding to the unpaired electron in cerium(III), the electron−nuclear interaction is likely to be the dominant factor in peak broadening and shifting. Furthermore, we expect peak broadening to increase as ^{1}H atoms get closer to the unpaired electron. For the ^{1}H atoms closest to the electron, peak broadening may make the NMR signal difficult to detect; for example, in Figure 4c, we see a "baseline roll" between 3.0 and 3.2 ppm, suggesting the presence of very broad NMR signals. Hence, the changes to the ^{1}H chemical shifts of the residues that are closer to the cerium(III) ion and directly participate in ion binding may be difficult to detect, creating what is known as "dark states" in NMR spectroscopy.[47] The peak broadening and shifting we highlight in Figure 4a,c,e are more detectable because they correspond to weaker electron−nuclear interactions, providing information about the residues that may not directly participate in cerium(III) binding and are farther from the binding site. We interpret the peak broadening in Figure 4a,c,e to be a result of multisite occupancy between structural conformations that produce multiple peaks per atomic site (although they may overlap). In Figure 4a, we observe peak splitting rather than peak broadening at 1.2 ppm because the

https://doi.org/10.1021/acsami.3c17565
ACS Appl. Mater. Interfaces 2024, 16, 16912−16926

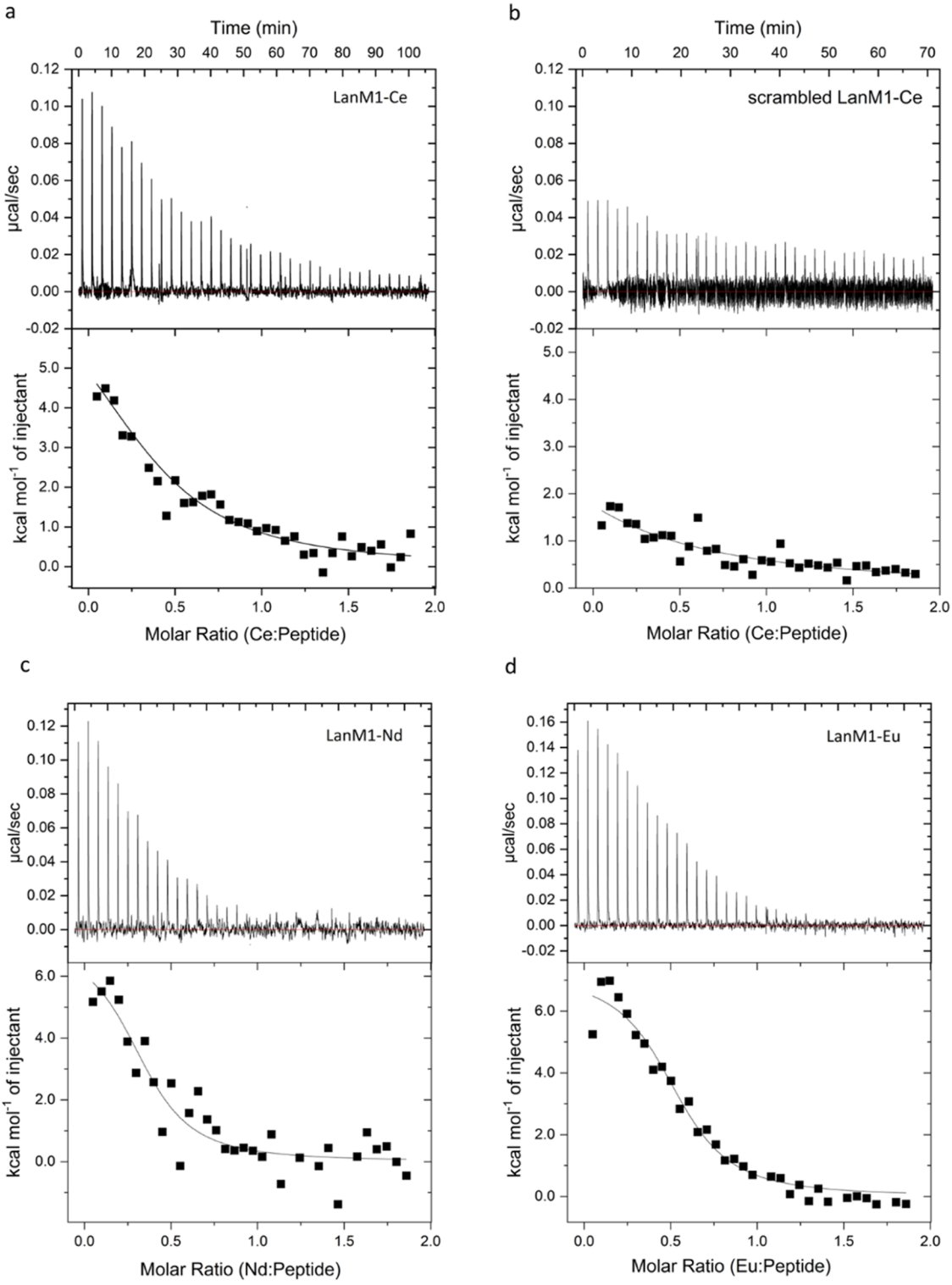

Figure 5. ITC raw data, Wiseman plot, and one-site binding model fit for (a) LanM1 with cerium(III) ions, (b) scrambled LanM1 with cerium(III) ions, (c) LanM1 with neodymium(III) ions, and (d) LanM1 with europium(III) ions. In all experiments, the peptides were in the cell at 20.0 μM and the ions were in the syringe at a concentration 200.0 μM. The experiments were performed at 30 °C using ultrapure water at a pH of ~4.5.

peptide adopts two different conformations with a larger chemical shift difference and no spectral overlap. The phenomenon of "pseudocontact shifts" induced by lanthanides is likely to be relevant here.[48−50] The emergence of a new peak in Figure 4e indicates a new conformation that occurs only in the presence of the cerium(III) ion. Further NMR experiments can provide more information about the precise interactions involved between the peptide residues and cerium(III) ions. Overall, our data support the conclusion that LanM1 binds to cerium(III), confirming CD and MD simulation results. In contrast, scrambled LanM1 has the same side chains as LanM1 but does not bind cerium(III), indicating the importance of the amino acid sequence.

https://doi.org/10.1021/acsami.3c17565
ACS Appl. Mater. Interfaces 2024, 16, 16912−16926

Table 1. Estimated Thermodynamic Properties for LanM1 Binding with Cerium(III), Neodymium(III), and Europium(III) Ions Using Isothermal Titration Calorimetry (ITC)[a]

peptide	REE ion	association constant K_a (μM^{-1})	dissociation constant K_d (μM)	ΔH (kcal/mol)	ΔS(cal/(mol K))	ΔG (kcal/mol)
LanM1	Ce	0.30 ± 0.13	3.84 ± 1.47	6.66 ± 1.32	46.85 ± 3.54	−7.50 ± 0.31
LanM1	Nd	0.70 ± 0.03	1.44 ± 0.07	6.10 ± 1.51	48.15 ± 3.04	−8.09 ± 0.03
LanM1	Eu	1.47 ± 0.80	0.80 ± 0.48	6.84 ± 5.09	50.60 ± 0.57	−8.49 ± 0.34
scrambled LanM1	Ce	0.05 ± 0.01	20.59 ± 5.84	13.11 ± 4.74	64.63 ± 15.61	−6.47 ± 0.25

[a]Results for scrambled LanM1 with cerium(III) are also reported. The experiments were conducted at 30 °C, and pH was ∼4.5. Data are represented by the average ± the standard deviation for n = 3 repeats.

Thermodynamic Properties of Binding in Solution. To better understand and elucidate the binding affinity, isothermal titration calorimetry was conducted to estimate the thermodynamic properties of binding for various REEs (Ce(III), Nd(III), Eu(III), and Y(III)) at 303.15 K. In addition, experiments on scrambled LanM1 with cerium(III) ions were conducted to serve as a comparison. Figure 5a,b shows the cerium titration curves (raw data), isotherm, and one-site binding model fit for LanM1 and scrambled LanM1, respectively. The titration results for neodymium and europium ions with LanM1 are provided in Figure 5c,d, respectively. LanM1 had a low affinity for Y(III) ions, making thermodynamic properties difficult to estimate. ITC raw data, the Wiseman plot, and one-site binding model fit for yttrium with LanM1 are provided in Figure S3.

At a given temperature, the change in enthalpy (ΔH) and change in entropy (ΔS) determine the sign and magnitude of the binding free energy using the expression $\Delta G = \Delta H - T\Delta S$. The estimated thermodynamic properties of binding for Ce(III), Nd(III), and Eu(III) with LanM1 and Ce(III) with the scrambled LanM1 are reported in Table 1. In the case of cerium(III) binding with LanM1, the changes in enthalpy (ΔH) and entropy (ΔS) were measured to be 6.66 ± 1.32 kcal/mol and 46.85 ± 3.54 cal/(mol K), respectively, and used to obtain the binding free energy (ΔG) of −7.50 ± 0.31 kcal/mol. The dissociation constant K_d was estimated to be 3.84 ± 1.47 μM, which is comparable to similar investigations of cerium(III) via ITC using a different peptide sequence that was derived from calmodulin.[16,24,51] A negative ΔG is an indication of spontaneous binding. The process is enthalpically disfavored, with the increase in entropy driving the process. For scrambled LanM1, K_d was estimated to be 20.59 ± 5.84 μM, nearly an order of magnitude higher.

The obtained K_d values for neodymium and europium ions with LanM1 were 1.44 ± 0.07 and 0.80 ± 0.48 μM, respectively. The dissociation constants were correlated to the ionic radius of REEs as shown in Figure S4, where K_d increases as the ionic radius increases. Nitz et al.[52] studied the binding affinity of REEs with lanthanide-binding tags (LBTs) and found a non-monotonic change in K_d with the ionic radius. The minimum K_d of 57 ± 3 nM was observed for Tb(III) that has an atomic radius of ∼1.04 A. In the light REE range, the K_d increased with the ionic radius, consistent with our results. Similar results were found in the calmodulin protein.[53]

The ITC results for the potential competitor ions calcium (Ca(II)) and copper (Cu(II)) with LanM1 are reported in Figure S5. It was found that LanM1 does not bind with copper and calcium ions, consistent with the similar investigation in which lanmodulin protein was immobilized onto agarose microbeads and was studied for its affinity toward several REEs and non-REEs by Dong et al.[22] In an investigation of the four EF-hand loop peptides of the lanmodulin protein by Gutenthaler et al.,[24] the peptide showed no affinity toward the calcium ion. In a study by Hussain et al.[21] of a thermoresponsive genetically encoded elastin-like polypeptide that has an REE-binding domain (lanmodulin), it was found that the polypeptide did not bind to copper and zinc ions, further supporting our findings. The results are also in agreement with Wei and co-workers[23] who found that lanmodulin protein immobilized to magnetic nanoparticles (MNP-LanM) did not adsorb non-REEs.

We also tested LanM1 binding affinity with cerium(III) at low-pH conditions. The studies at low-pH conditions are relevant to coal mine drainages where the discharges are at low pH (<5).[54] ITC experiments at three pH conditions, 2.0, 3.0, and 3.5, were performed (Figure S6). It was found that there was no binding at pH 2.0. However, the titration curves at pH 3.0 and 3.5 show increasingly distinct changes in energy during the first few injections, indicating increasing binding affinity. This suggests that free peptide could be regenerated by lowering the pH to release the ions. In recent work by Dong et al.,[22] desorption studies were performed on agarose beads with grafted lanmodulin protein in which the effect of pH was investigated. It was found that immobilized lanmodulin can effectively bind Nd(III) ions down to pH 2.4. However, further lowering the pH to 2.2 resulted in a 50% drop in binding, and it became insignificant below pH 1.7. Our results also agree with Deblonde et al.,[19] who showed that solubilized lanmodulin protein retains REE binding affinity down to around pH 2.5. The pK_a values of aspartic acid and glutamic acid are ∼3.9 and ∼4.3, respectively, so below this pH range, the peptide loses its negatively charged groups and might contribute to low affinity for REEs below pH 2.5. Finally, it was observed that affinity is generally higher at pH 5.5 compared to pH 4.5, but the trend in affinity with ionic radius is maintained (Table S4).

Binding Analysis of Immobilized Peptides. To understand the binding affinity of the immobilized peptide with some REEs and competing non-REEs, a quartz crystal microbalance with dissipation (QCM-D) analysis was performed. In a typical QCM-D experiment, ultrapure water is introduced on the gold sensor to generate a baseline. Once a stable baseline is established, peptide solution of known concentration is introduced, and a negative shift in frequency is observed, which is proportional to the hydrated mass loading of the peptide on the surface. Rinses are often employed to remove weakly bound molecules. In addition to frequency, dissipation is measured, which provides information about the energy loss and gives an indication of the viscoelastic properties. If there is no significant shift in dissipation, the layer is rigid; otherwise, the layer is viscoelastic.[55] After the desired peptide is immobilized on the gold surface and an ultrapure water rinse is performed, REE binding on the immobilized peptide is done by allowing an REE solution of known concentration to flow over the surface. Then, another round of ultrapure water rinsing is performed to remove weakly bound REEs. In this study, the amount of REE

https://doi.org/10.1021/acsami.3c17565
ACS Appl. Mater. Interfaces 2024, 16, 16912−16926

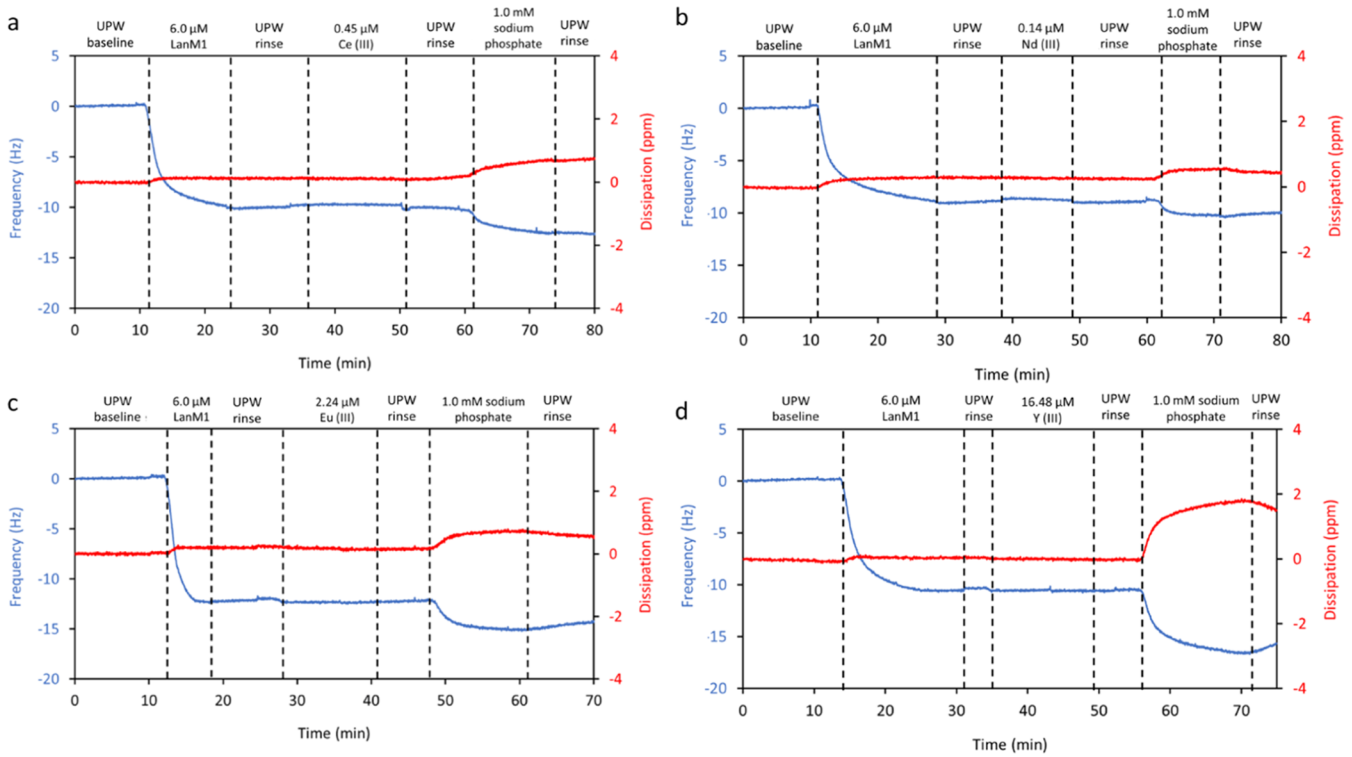

Figure 6. Frequency and dissipation shifts measured using a quartz crystal microbalance (QCM-D) for (a) cerium(III), (b) neodymium(III), (c) europium(III), and (d) yttrium(III) adsorption on LanM1. The dashed lines show when the solution was changed, and the labels within the lines show the solution during that time. The blue line corresponds to the frequency shift, and the red line corresponds to the dissipation shift. The 9th overtones are shown. The pH in these experiments is ~5.5.

that binds to the peptide is not enough to illicit a significant shift in frequency. Therefore, after ultrapure water rinsing, a 1 mM sodium phosphate solution is allowed to flow over the surface and bind to surface-bound REEs as a way to quantify the amount of REEs bound. This technique using phosphate was confirmed by using it to estimate the K_d of a peptide derived from calmodulin and was found to be similar to our previous work (Figure S7[16]). During LanM1 peptide loading, there were no significant changes in dissipation observed, resulting in a rigid layer formation, and thus, the Sauerbrey model was sufficient to estimate the mass loading. However, a viscoelastic layer was formed upon phosphate loading and the Voigt model[56] was used to estimate the mass loading.

All surface binding studies were conducted, assuming that the peptide binding to REEs was a reversible process, as shown by eq 1

$$\text{peptide} + \text{REE} \underset{k_f}{\overset{k_r}{\rightleftharpoons}} \text{peptide-REE} \tag{1}$$

where k_f represents the forward rate constant and k_r is the reverse rate constant. The binding affinity K_d is then defined as the ratio k_r/k_f. K_d is a dissociation constant and is the reciprocal of the association constant K_a that is often reported for ligand−ion complexation. The linearized slope of binding for a peptide−REE−phosphate system, as shown in Note S1, is found to be identical to that of a peptide−REE system. When tested with calmodulin peptides, we see that the K_d estimated from phosphate addition was 1.6 μM as shown in Figure S7, which is around what was previously reported (1.3 μM[16]). We assume that the amount of phosphate bound is proportional to the amount of cerium bound on the surface of the QCM sensor. To ensure that phosphate does not interact with the lanmodulin peptides, control experiments were conducted, where no binding was observed, as shown in Figure S8. Our previous study shows that when no peptide was present on the QCM sensor, no irreversible binding was observed for phosphate,[17] indicating that all phosphate binding seen is due to interactions with peptide−cerium films. We also observed that higher LanM1 loading on gold sensors (frequency change of ~15 Hz or greater) will result in minimal REE binding as shown in Figure S9. Thus, it is critical to control the loading of the peptide on the surface to maintain peptide affinity. This observation suggests that the density of the peptides on a surface plays a role in ion binding. In solution, the peptides are freely suspended at low concentrations, whereas peptides tethered to a surface or particle are more crowded and we speculate that the crowding of peptides on a surface may cause changes in the peptide secondary structure, thereby altering the binding pocket, changes to water organization around the peptide, steric hindrance, or interaction of peptides with each other. Therefore, depending on the peptide density on the surface, the trends in peptide−ion affinity may be different for a surface-immobilized peptide than a peptide in solution. Any changes to trends in affinity will manifest in the peptide selectivity for REEs over non-REEs or one REE over another.

Figure 6a−d shows QCM-D results for gold-immobilized LanM1 exposed to Ce(III), Nd(III), Eu(III), and Y(III) ions, respectively. Figure 6 displays experiments performed at the lowest REE concentrations where binding was observed, where the blue line corresponds to the frequency shift, while the red line corresponds to the dissipation shift. Ultrapure water served as the baseline for the experiment, which was immediately followed by a 6.0 μM peptide solution. An experiment exposing

https://doi.org/10.1021/acsami.3c17565
ACS Appl. Mater. Interfaces 2024, 16, 16912−16926

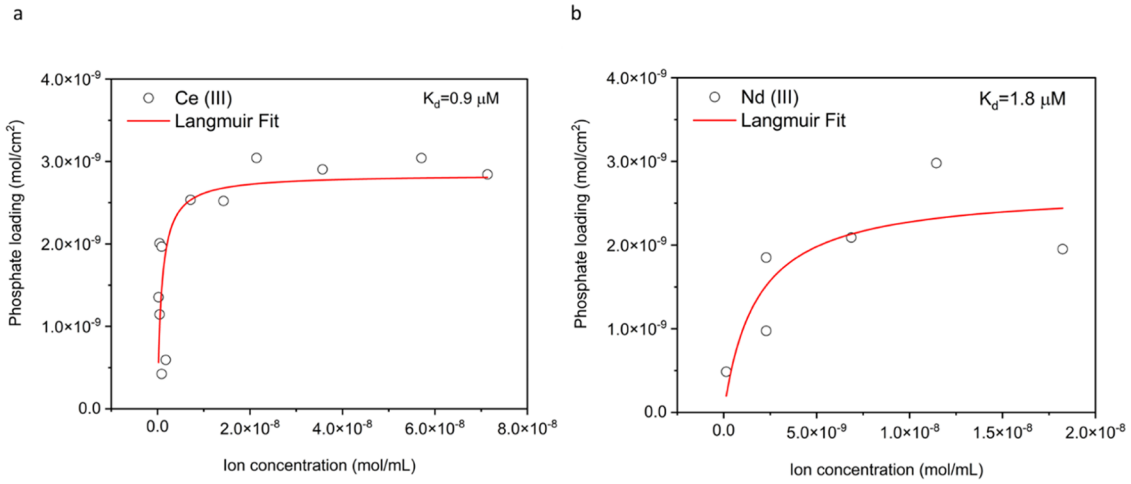

Figure 7. Binding of (a) Ce(III) and (b) Nd(III) ions to gold-immobilized LanM1 peptides, where phosphate is proportional to REE binding. In both cases, a simple Langmuir adsorption model was fit to estimate the K_d. Open circles represent experimental data points, whereas the red lines show the Langmuir fit. Estimated K_d values are shown in the respective panels. The pH in these experiments is ~5.5.

gold-immobilized scrambled LanM1 to Ce(III) is shown in Figure S10. In the case of LanM1 and scrambled LanM1, a frequency shift upon addition of phosphate ions was observed down to 0.45 μM Ce(III), with much less binding occurring in the case of the scrambled LanM1. These results are consistent with bulk investigations using CD, NMR, ITC, and molecular dynamics results showing scrambled LanM1 having a lower affinity for cerium(III) than that of LanM1. In the case of Nd(III), Eu(III), and Y(III), the lowest concentration binding was observed at 0.14, 2.24, and 16.48 μM, respectively.

Non-REE ions are also known to complex with phosphate, and when using the solubility product constant as an rough indication of the affinity of the ions for phosphate, Ca(II) and Cu(II) will have at least as high of an affinity when compared to cerium(III).[57] Therefore, similar QCM-D experiments were performed with two non-REE Ca(II) and Cu(II) competitor ions. The results of the surface-bound LanM1 peptide with these ions are provided in Figure S11. Like the bulk, the LanM1 peptide does not show affinity for either calcium or copper ions. Even at a higher competitor ion concentration of 29.0 μM, no change in the frequency was observed.

QCM-D experiments were performed at various REE ion concentrations to estimate surface-bound LanM1 dissociation constants for Ce(III) and Nd(III). In acid mine drainage, the concentration of Ce(III) and Nd(III) is the highest among other REEs,[58] which makes this pair a particular interest for that application. The Langmuir adsorption isotherm model was fit to phosphate loading data at different REE concentrations in QCM-D experiments to describe the adsorption process.[59,60] Although, it is an ideal model that may not fully capture the complexity of adsorption, it can still provide valuable insights into the adsorption behavior. The model is given as

$$q_e = \frac{R_T C_e}{C_e + K_d} \quad (2)$$

where q_e is the phosphate loading (mol/cm^2), R_T (mol/cm^2) is the Langmuir constant related to the maximum phosphate loading, K_d (mol/mL) is the dissociation constant, and C_e (mol/mL) is the equilibrium bulk concentration of the ions. In this work, nonlinear regression was performed using OriginLab software to fit the data. The removal of one outlier was allowed for each ion dataset.

Figure 7 shows the change in phosphate loading (proportional to REE loading) with ion concentration for cerium(III) and neodymium(III) along with Langmuir fitting. Surface-bound LanM1 dissociation constants (K_d) of ~0.9 and ~1.8 μM were obtained for cerium(III) and neodymium(III), respectively. Details of the nonlinear fitting are provided in Table S1. When compared with the bulk results at similar pH of 5.5 (see Table S4), it is found that the affinity for cerium(III) ions remains approximately the same under the conditions of the QCM experiment. Because of the high error, it is difficult to determine if there is a shift for Nd(III) upon peptide immobilization. However, these results show for the first time that surface-bound LanM1 peptides bind REEs, which motivates future studies to explore how immobilization impacts the trends in K_d.

Selectivity Analysis of Immobilized Peptides. In a practical separation scheme, immobilized peptides are exposed to a mixture of REEs. Separation occurs if the peptide has a higher affinity (lower K_d) for one REE over another due to the preferential partitioning of the REE ion onto the solid peptide-containing phase. For dilute solutions, selectivity can be approximated using a ratio of association constants ($K_a = 1/K_d$) where the ideal selectivity is represented as $\alpha_{1/2} = K_{a1}/K_{a2}$ and 1 and 2 represent different metal species.[61] Since $\alpha_{1/2}$ is based on the association reaction, $\alpha_{1/2} > 1$ indicates a higher affinity for species 1. Higher values of $\alpha_{1/2}$ indicate higher degrees of separation between the two ions. The selectivities of the LBT peptide, LanM protein, and LanM1 peptide for Nd over Ce are summarized in Table 2. Typically, selectivity for neighboring lanthanides is analyzed; however, the Nd/Ce ion pair was selected to enable the comparison with this work. Two nonbiological ligands are included as these are the leading commercial extractive resins for REE separations: DGA-linear and DGA-branched (Eichrom Technologies, Ltd.). A key distinguishing factor between the bioderived ligands and the DGAs is the solution conditions under which selectivity is achieved. DGA-linear and DGA-branched resins exhibit selectivity for one REE over another REE at high acid concentrations < pH 1, whereas the bioderived ligands exhibit selectivity in more moderate pH solutions, i.e., >pH 3. The K_a, k', and K_d values used to construct Table 2 are given in Tables S2 and S3 of the Supporting Information.

https://doi.org/10.1021/acsami.3c17565
ACS Appl. Mater. Interfaces 2024, 16, 16912−16926

Table 2. Calculated Ideal Selectivity for DGA Resins, LBT Peptide, LanM Protein, and LanM1 Peptide for Selected REE Pairs[a]

ligand, support	matrix	ion pair	selectivity (K_{a1}/K_{a2}) or (k'_1/k'_2)	K_a or k' refs
DGA-branched, resin	1 M HNO_3	Nd/Ce	1.8	Horwitz[62]
DGA-linear, resin	0.05 M HNO_3	Nd/Ce	4.1	Horwitz[62]
LanM protein, unsupported	pH 5, 100 mM KCl	Nd/Pr	0.5	Deblonde[b19]
LBT, unsupported	pH 7.0, 10 mM HEPES, 100 mM NaCl	Nd/Ce	3.5	Nitz[52]
LanM1, unsupported	pH ~5.5, ultrapure water	Nd/Ce	2.0	this work
LanM1, on gold	pH ~5.5, ultrapure water	Nd/Ce	0.5	this work

[a]k' is proportional to the K_a. [b]Ce data was not available; therefore, Pr selectivity is reported instead.

A common challenge when comparing association and dissociation constants (K_a and K_d) across the literature is the wide variation of matrices used for binding (pH, ionic strength, buffer, or acid type) and the ions tested. For this reason, the discussion herein will refer to general trends and order of magnitude differences, recognizing the caveat that the lanmodulin protein data in Table 2 represent a more challenging separation of neighbors Nd/Pr than Nd/Ce—immobilized LanM1 peptides exhibit selectivity that is on par with the LanM protein at 0.5. This is interesting because the K_d of the LanM protein is 6 orders of magnitude lower than that of LanM1 peptides. We recall that the K_d for LanM protein across the lanthanide series ranges from 0.4 to 10 pM,[19] and the K_d for immobilized LanM1 in this work ranges from 0.9 to 1.8 μM. Thus, high affinity does not necessarily correlate to high selectivity between the tested REEs.

Common ligands for lanthanide separations such as EDTA, DOTA, and DTPA exhibit a monotonic increase in affinity as the atomic number and charge density increase across the lanthanide series[63] known as the size selectivity trend. Specialty macrocyclic ligands like Macropa exhibit a reverse size selectivity trend where the affinity decreases monotonically as the atomic number and charge density increase across the lanthanide series.[64] The lanmodulin protein exhibits a dual selectivity in which an inflection point in the dissociation constant occurs at Sm. The selectivity trend of the LBT peptide is more consistent with that of the traditional ligands as the affinity increases with increasing atomic number for the light lanthanides La → Eu. The LBT peptide shows negligible selectivity between the heavier lanthanides Eu → Lu. Based on the first three lanthanides tested in this series, the LanM1 peptide exhibits the traditional size selectivity trend in solution, Table 1. Further investigation of dissociation constants with heavier lanthanides will be necessary to discern the full extent of the selectivity trend for LanM1 in solution. Based on the first two tested lanthanides (Nd and Ce) for immobilized LanM1, the selectivity trends of the peptide tethered to surfaces may warrant further investigation.

Binding Investigation on Gold Nanoparticles (GNPs). The potential to use surface-bound LanM1 in REE separation is demonstrated by immobilizing the LanM1 peptide on gold nanoparticles (diameter of < 100 nm) and subsequently estimating the adsorption capacity of peptide-immobilized GNPs as shown in Figure 8a.

After peptide functionalization, GNPs were incubated with REE-containing solution, and then, the GNPs were separated from the supernatant and titrated with Arsenazo III reagent. The

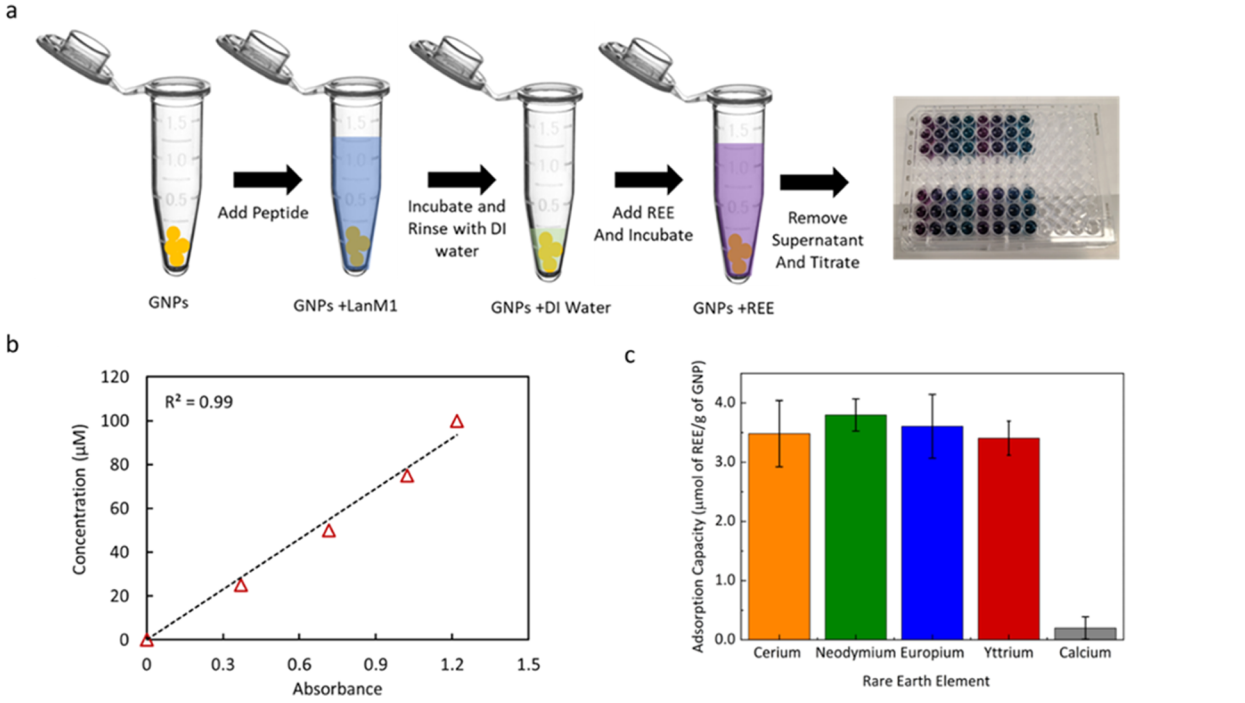

Figure 8. (a) Pictorial representation of the step-by-step procedure used to make peptide-bound gold nanoparticles (GNPs) and analyze REE binding capacity. (b) Calibration curve for Ce(III) ions based on the UV−visible absorption spectra. (c) Comparison of the adsorption capacities (μmol REE/g GNP-LanM1) for different REEs and negligible adsorption of calcium(II) ions.

https://doi.org/10.1021/acsami.3c17565
ACS Appl. Mater. Interfaces 2024, 16, 16912−16926

absorption at 655 nm wavelength was measured and used to generate a calibration curve like that shown in Figure 8b, from which the concentration of the sample supernatant was estimated. Figure 8b shows an example calibration curve for Ce(III) ions, and calibration curves for Nd(III), Eu(III), and Y(III) and Ca(II) ions can be found in Figure S12. UV−visible absorption spectra of known cerium concentration solutions titrated against Arsenazo III reagent used to generate the calibration curve are provided in Figure S13.

The adsorption capacity (μmol REE/g of GNP-LanM1) was calculated using eq 3

$$Q_e = \frac{(C_0 - C_e) \times V}{m} \quad (3)$$

where C_0 is the initial REE concentration (μM); C_e is the REE concentration of the supernatant; V is the volume in the vial (L); and m is the mass of the GNP-LanM1 (g).

Several equilibrium adsorption experiments of LanM1-GNPs at different concentrations were performed for REEs Ce(III), Nd(III), Eu(III), and Y(III) and non-REEs Ca(II) and the estimated adsorption capacity for the ions at different concentrations is reported in Table S5. A comparison of average equilibrium adsorption capacities of REEs and competing non-REE calcium(II) ions is shown in Figure 8c. These values for REEs are assumed to be the saturated adsorption capacity, since saturation appears to occur at concentrations tested (see Table S5). The results show that LanM1-grafted GNPs do not adsorb calcium ions. These findings align well with ITC and QCM-D results in this study and are consistent with similar investigations.[22,24] The REE-saturated adsorption capacities of GNP-grafted LanM1 for Ce(III), Nd(III), Eu(III), and Y(III) are similar, ∼3.5 μmol REE per gram of GNP-LanM1, further supporting that the concentration range is above the saturation point for these REE ions.

In a recent study of lanmodulin-functionalized magnetic nanoparticles for REE recovery, a saturated adsorption capacity of 5.46 ± 0.46 μmol Tb/g of MNP was reported. The experiment was performed using 20 mM 2-(*N*-morpholino)-ethanesulfonic acid (MES) buffer at pH 5.0 with 2.5 mg/mL MNP-LanM and ∼62.93 μM Tb(III),[23] which has some similarities to our experiment in DI water at pH 5.0−5.5 with 5−8 mg GNP/mL and 20−125 μM REE, serving as a useful comparison. In their study, the loading on MNPs was 2.67 ± 0.15 μmol LanM SpyCatcher/g-MNP. We roughly estimated the molar loading of LanM1 to be ∼3.74 μmol LanM1/g-GNP based on our QCM-D mass estimates, noting that our estimate is likely and overestimated because we did not account for water. The results in the QCM-D experiment show a minimum dissipation during peptide loading, which indicates a rigid layer formation and low water content; however, the degree of hydration of the layer is unknown. Nonetheless, the molar peptide loading on GNPs is of similar order of magnitude to that of the SpyCatcher MNPs. When adsorbing in a monolayer, the molar surface density of peptides is expected to be higher than the bulkier proteins due to the smaller size.[65] However, in this case, the comparison is made between the monolayer of the LanM1 peptide and lanmodulin protein immobilized on the branched polymer (SpyCatcher) functionalized on MNPs. The branched polymer provides a three-dimensional scaffold onto which the proteins can be conjugated, whereas the peptides were directly conjugated to the gold nanoparticle surface in a monolayer. The three-dimensional structure of the brushes provides additional capacity per unit surface area of the underlying MNP. In addition, the lanmodulin protein has more available REE binding sites per mole than the LanM1 peptide, thus resulting in an appropriately lower saturated binding capacity for the material in this study. One study had shown that immobilized lanmodulin protein had two sites available for REE binding in comparison to three in the solution.[22] The study suggested the inaccessibility of one site upon immobilization. We note that our estimated molar loading of peptide is close to the saturated adsorption capacity measured of ∼3.5 μmol REE/g of GNP-LanM1, indicating high site accessibility. Lanmodulin protein has a molecular weight that is ∼7 times higher than that of the LanM1 peptide, indicating that the maximum adsorption capacity achieved with the peptide is relatively high when considering the mass of peptide used compared to the lanmodulin-MNP material. While this comparison is useful, we note that it is difficult to compare the two studies because adsorption capacity can depend on several factors.[66]

CONCLUSIONS

In summary, LanM1 peptide derived from the EF-hand loop 1 of lanmodulin was tested for its binding affinity for different REEs, Ce(III), Nd(III), Eu(III), and Y(III), both in the bulk and when bound to a gold surface using both experimental and computational techniques. The ability of Ce(III) ions to bind with LanM1 and scrambled LanM1 was confirmed using circular dichroism (CD) and corroborated using molecular dynamics and nuclear magnetic resonance spectroscopy (NMR) analysis. Isothermal titration calorimetry (ITC) results showed spontaneous binding of all REEs to the LanM1 peptide. The binding was enthalpically disfavored but was driven by a positive change in entropy. The dissociation constants from ITC were correlated to the ionic radius of REEs with a K_d of 3.84 ± 1.47, 1.44 ± 0. 07, and 0.80 ± 0.48 μM for Ce(III), Nd(III), and Eu(III), respectively at pH ∼4.5. In the case of non-REE ions, calcium Ca(II) and Cu(II), no affinity with LanM1 was observed. At pH below 2, Ce(III) was not observed to bind with LanM1, suggesting a pH swing as a possible regeneration mechanism. Quartz crystal microbalance with dissipation (QCM-D) analysis was performed to characterize the binding of REEs and non-REEs to surface-immobilized LanM1. The dissociation constants obtained from Langmuir model fitting suggested that the binding affinities for Ce(III) and Nd(III) with surface-bound LanM1 were estimated to be roughly ∼0.9 and 1.8 μM, respectively at pH ∼5.5. The saturated adsorption capacity of LanM1 immobilized on gold nanoparticles was estimated using Arsenazo III-based colorimetric dye displacement assay and ultraviolet−visible (UV−vis) spectrophotometry to be around 3.5 μmol REE/mg of GNP-LanM1, with negligible binding to Ca(II) ions. Overall, this study demonstrates the potential for surface-bound LanM1 peptides to have a high affinity for REEs and be used in advanced separation technologies. The work also motivates future studies to investigate how immobilizing this peptide might impact trends in REE affinity and how the LanM1 peptide sequence might be manipulated to optimize the separation of REE mixtures.

ASSOCIATED CONTENT

Supporting Information

The Supporting Information is available free of charge at https://pubs.acs.org/doi/10.1021/acsami.3c17565.

https://doi.org/10.1021/acsami.3c17565
ACS Appl. Mater. Interfaces 2024, 16, 16912−16926

Snapshot of the molecular dynamics system, NMR results, ITC results, QCM-D results, Scatchard plot, Langmuir model regression data, summary of adsorption metrics used in the selectivity analysis, estimated adsorption capacities for REEs using GNPs, and derivation for a two-step Scatchard analysis. A repository of the GROMCAS input files is created on GitHub: https://github.com/gev28/Gromacs_input_file (PDF)

AUTHOR INFORMATION

Corresponding Author

Julie Renner − *Department of Chemical and Biomolecular Engineering, Case Western Reserve University, Cleveland, Ohio 44106, United States;* orcid.org/0000-0002-6140-4346; Email: jxr484@case.edu

Authors

Geeta Verma − *Department of Chemical and Biomolecular Engineering, Case Western Reserve University, Cleveland, Ohio 44106, United States;* orcid.org/0000-0002-4882-950X

Jacob Hostert − *Department of Chemical and Biomolecular Engineering, Case Western Reserve University, Cleveland, Ohio 44106, United States;* orcid.org/0000-0003-3519-7002

Alex A. Summerville − *Department of Chemical and Biomolecular Engineering, Case Western Reserve University, Cleveland, Ohio 44106, United States*

Alicia S. Robang − *School of Chemical and Biomolecular Engineering, Georgia Institute of Technology, Atlanta, Georgia 30332, United States;* orcid.org/0000-0003-3857-9559

Ricardo Garcia Carcamo − *Department of Chemical and Biomolecular Engineering, Ohio State University, Columbus, Ohio 43210, United States*

Anant K. Paravastu − *School of Chemical and Biomolecular Engineering, Georgia Institute of Technology, Atlanta, Georgia 30332, United States; Parker H. Petit Institute for Bioengineering and Biosciences, Georgia Institute of Technology, Atlanta, Georgia 30332, United States;* orcid.org/0000-0001-7183-1942

Rachel B. Getman − *Department of Chemical and Biomolecular Engineering, Ohio State University, Columbus, Ohio 43210, United States;* orcid.org/0000-0003-0755-0534

Christine E. Duval − *Department of Chemical and Biomolecular Engineering, Case Western Reserve University, Cleveland, Ohio 44106, United States;* orcid.org/0000-0002-8630-5483

Complete contact information is available at: https://pubs.acs.org/10.1021/acsami.3c17565

Author Contributions

[⊥]G.V. and J.H. contributed equally to this work.

Notes

The authors declare no competing financial interest.

ACKNOWLEDGMENTS

The authors thank Molecular Biotechnology Core at Cleveland Clinic and thank Dr. Smarajit Bandyopadhyay, Director, Molecular Biotechnology Core, for his help with CD and ITC experiments. A special thanks to Sayani Biswas, a graduate student in the Department of Chemical and Biomolecular Engineering at Ohio State University, for validating MD calculations. The authors also thank Dr. Jeffrey Capadona, a professor in the Department of Biomedical Engineering at Case Western Reserve University, for allowing us to use QCM-D instrument in his lab. This work used the Extreme Science and Engineering Discovery Environment (XSEDE), which is supported by the National Science Foundation grant number ACI-1548562. Specifically, it used the Bridges-2 system, which is supported by the NSF award number ACI-1928147, at the Pittsburgh Supercomputing Center (PSC). The project is supported by the National Science Foundation ECO−CBET program, award #2133549. The authors also acknowledge the use of instruments at the NMR center at the Georgia Institute of Technology.

REFERENCES

(1) Hossain, M. K.; Raihan, G. A.; Akbar, M. A.; Rubel, M. H. K.; Ahmed, M. H.; Khan, M. I.; Hossain, S.; Sen, S. K.; Jalal, M. I. E.; El-Denglawey, A. Current Applications and Future Potential of Rare Earth Oxides in Sustainable Nuclear, Radiation, and Energy Devices: A Review. *ACS Appl. Electron. Mater.* **2022**, *4* (7), 3327−3353.

(2) Elbashier, E.; Mussa, A.; Hafiz, M.; Hawari, A. H. Recovery of rare earth elements from waste streams using membrane processes: An overview. *Hydrometallurgy* **2021**, *204*, No. 105706.

(3) Ni'am, A. C.; Wang, Y.-F.; Chen, S.-W.; Chang, G.-M.; You, S.-J. Simultaneous recovery of rare earth elements from waste permanent magnets (WPMs) leach liquor by solvent extraction and hollow fiber supported liquid membrane. *Chem. Eng. Process.* **2020**, *148*, No. 107831.

(4) Murthy, Z.; Choudhary, A. Separation of cerium from feed solution by nanofiltration. *Desalination* **2011**, *279* (1−3), 428−432.

(5) Fritz, J. S. Early milestones in the development of ion-exchange chromatography: a personal account. *J. Chromatogr. A* **2004**, *1039* (1), 3−12.

(6) Hassas, B. V.; Rezaee, M.; Pisupati, S. V. Effect of various ligands on the selective precipitation of critical and rare earth elements from acid mine drainage. *Chemosphere* **2021**, *280*, No. 130684.

(7) Park, D.; Middleton, A.; Smith, R.; Deblonde, G.; Laudal, D.; Theaker, N.; Hsu-Kim, H.; Jiao, Y. A biosorption-based approach for selective extraction of rare earth elements from coal byproducts. *Sep. Purif. Technol.* **2020**, *241*, No. 116726.

(8) Castrillejo, Y.; Bermejo, M. R.; Pardo, R.; Martínez, A. M. Use of electrochemical techniques for the study of solubilization processes of cerium−oxide compounds and recovery of the metal from molten chlorides. *J. Electroanal. Chem.* **2002**, *522* (2), 124−140.

(9) Mwewa, B.; Tadie, M.; Ndlovu, S.; Simate, G. S.; Matinde, E. Recovery of rare earth elements from acid mine drainage: A review of the extraction methods. *J. Environ. Chem. Eng.* **2022**, *10* (3), No. 107704.

(10) Chen, Z.; Li, Z.; Chen, J.; Kallem, P.; Banat, F.; Qiu, H. Recent advances in selective separation technologies of rare earth elements: a review. *J. Environ. Chem. Eng.* **2022**, *10* (1), No. 107104.

(11) Bashiri, A.; Nikzad, A.; Maleki, R.; Asadnia, M.; Razmjou, A. Rare Earth Elements Recovery Using Selective Membranes via Extraction and Rejection. *Membranes* **2022**, *12* (1), No. 80.

(12) Ambaye, T. G.; Vaccari, M.; Castro, F. D.; Prasad, S.; Rtimi, S. Emerging technologies for the recovery of rare earth elements (REEs) from the end-of-life electronic wastes: a review on progress, challenges, and perspectives. *Environ. Sci. Pollut. Res.* **2020**, *27* (29), 36052−36074.

(13) Braun, R.; Bachmann, S.; Schönberger, N.; Matys, S.; Lederer, F.; Pollmann, K. Peptides as biosorbents − Promising tools for resource recovery. *Res. Microbiol.* **2018**, *169* (10), 649−658.

(14) Wallin, C.; Kulkarni, Y. S.; Abelein, A.; Jarvet, J.; Liao, Q.; Strodel, B.; Olsson, L.; Luo, J.; Abrahams, J. P.; Sholts, S. B.; Roos, P. M.; Kamerlin, S. C. L.; Gräslund, A.; Wärmländer, S. K. T. S. Characterization of Mn(II) ion binding to the amyloid-β peptide in Alzheimers disease. *J. Trace Elem. Med. Biol.* **2016**, *38*, 183−193.

(15) Hatanaka, T.; Kikkawa, N.; Matsugami, A.; Hosokawa, Y.; Hayashi, F.; Ishida, N. The origins of binding specificity of a lanthanide ion binding peptide. *Sci. Rep.* **2020**, *10* (1), No. 19468.

(16) Xu, M.; Su, Z.; Renner, J. N. Characterization of cerium (III) ion binding to surface-immobilized EF-hand loop I of calmodulin. *Pept. Sci.* **2019**, *111* (6), No. e24133.
(17) Su, Z.; Hostert, J. D.; Renner, J. N. Phosphate Recovery by a Surface-Immobilized Cerium Affinity Peptide. *ACS ES&T Water* **2021**, *1* (1), 58−67.
(18) Cotruvo, J. A., Jr.; Featherston, E. R.; Mattocks, J. A.; Ho, J. V.; Laremore, T. N. Lanmodulin: A Highly Selective Lanthanide-Binding Protein from a Lanthanide-Utilizing Bacterium. *J. Am. Chem. Soc.* **2018**, *140* (44), 15056−15061.
(19) Deblonde, G. J. P.; Mattocks, J. A.; Park, D. M.; Reed, D. W.; Cotruvo, J. A.; Jiao, Y. Selective and Efficient Biomacromolecular Extraction of Rare-Earth Elements using Lanmodulin. *Inorg. Chem.* **2020**, *59* (17), 11855−11867.
(20) Xie, X.; Yang, K.; Lu, Y.; Li, Y.; Yan, J.; Huang, J.; Xu, L.; Yang, M.; Yan, Y. Broad-spectrum and effective rare earth enriching via Lanmodulin-displayed Yarrowia lipolytica. *J. Hazard. Mater.* **2022**, *438*, No. 129561.
(21) Hussain, Z.; Kim, S.; Cho, J.; Sim, G.; Park, Y.; Kwon, I. Repeated Recovery of Rare Earth Elements Using a Highly Selective and Thermo-Responsive Genetically Encoded Polypeptide. *Adv. Funct. Mater.* **2022**, *32* (13), No. 2109158.
(22) Dong, Z.; Mattocks, J. A.; Deblonde, G. J. P.; Hu, D.; Jiao, Y.; Cotruvo, J. A., Jr.; Park, D. M. Bridging Hydrometallurgy and Biochemistry: A Protein-Based Process for Recovery and Separation of Rare Earth Elements. *ACS Cent. Sci.* **2021**, *7* (11), 1798−1808.
(23) Ye, Q.; Jin, X.; Zhu, B.; Gao, H.; Wei, N. Lanmodulin-Functionalized Magnetic Nanoparticles as a Highly Selective Biosorbent for Recovery of Rare Earth Elements. *Environ. Sci. Technol.* **2023**, *57* (10), 4276−4285.
(24) Gutenthaler, S.; Tsushima, S.; Steudtner, R.; Gailer, M.; Hoffmann-Röder, A.; Drobot, B.; Daumann, L. LanM Peptides−Unravelling the Binding Properties of the EF-Hand Loop Sequences Stripped from the Structural Corset. *Inorg. Chem. Front.* **2022**, *9* (16), 4009−4021.
(25) Gerblinger, J.; Lohwasser, W.; Lampe, U.; Meixner, H. High temperature oxygen sensor based on sputtered cerium oxide. *Sens. Actuators, B* **1995**, *26* (1), 93−96.
(26) El Idrissi, B.; Addou, M.; Outzourhit, A.; Regragui, M.; Bougrine, A.; Kachouane, A. Sprayed CeO2 thin films for electrochromic applications. *Sol. Energy Mater. Sol. Cells* **2001**, *69* (1), 1−8.
(27) Charalampides, G.; Vatalis, K. I.; Apostoplos, B.; Ploutarch-Nikolas, B. Rare Earth Elements: Industrial Applications and Economic Dependency of Europe. *Procedia Econ. Finance* **2015**, *24*, 126−135.
(28) Patil, A. S.; Patil, A. V.; Dighavkar, C. G.; Adole, V. A.; Tupe, U. J. Synthesis techniques and applications of rare earth metal oxides semiconductors: A review. *Chem. Phys. Lett.* **2022**, *796*, No. 139555.
(29) Hossain, M. K.; Hossain, S.; Ahmed, M. H.; Khan, M. I.; Haque, N.; Raihan, G. A. A Review on Optical Applications, Prospects, and Challenges of Rare-Earth Oxides. *ACS Appl. Electron. Mater.* **2021**, *3* (9), 3715−3746.
(30) Humphrey, W.; Dalke, A.; Schulten, K. VMD: Visual molecular dynamics. *J. Mol. Graphics* **1996**, *14* (1), 33−38.
(31) Su, Z. H.; Pramounmat, N.; Watson, S. T.; Renner, J. N. Engineered interaction between short elastin-like peptides and perfluorinated sulfonic-acid ionomer. *Soft Matter* **2018**, *14* (18), 3528−3535.
(32) Van Der Spoel, D.; Lindahl, E.; Hess, B.; Groenhof, G.; Mark, A. E.; Berendsen, H. J. C. GROMACS: Fast, flexible, and free. *J. Comput. Chem.* **2005**, *26* (16), 1701−1718.
(33) Goddard, T. D.; Huang, C. C.; Meng, E. C.; Pettersen, E. F.; Couch, G. S.; Morris, J. H.; Ferrin, T. E. UCSF ChimeraX: Meeting modern challenges in visualization and analysis. *Protein Sci.* **2018**, *27* (1), 14−25.
(34) Brooks, B. R.; Bruccoleri, R. E.; Olafson, B. D.; States, D. J.; Swaminathan, S.; Karplus, M. CHARMM: A program for macromolecular energy, minimization, and dynamics calculations. *J. Comput. Chem.* **1983**, *4* (2), 187−217.
(35) Sinitsyn, A. V.; Gracheva, M. E. Atomistic model of a ceria nanoparticle with Ce(3 +) and Ce(4 +) atoms. *Nanotechnology* **2020**, *31* (31), No. 315708.
(36) Migliorati, V.; Serva, A.; Terenzio, F. M.; D'Angelo, P. Development of Lennard-Jones and Buckingham Potentials for Lanthanoid Ions in Water. *Inorg. Chem.* **2017**, *56* (11), 6214−6224.
(37) Li, P.; Song, L. F.; Merz, K. M., Jr. Parameterization of Highly Charged Metal Ions Using the 12−6-4 LJ-Type Nonbonded Model in Explicit Water. *J. Phys. Chem. B* **2015**, *119* (3), 883−895.
(38) Duan, L.; Liu, X.; Zhang, J. Z. H. Interaction Entropy: A New Paradigm for Highly Efficient and Reliable Computation of Protein−Ligand Binding Free Energy. *J. Am. Chem. Soc.* **2016**, *138* (17), 5722−5728.
(39) Hess, B.; Kutzner, C.; van der Spoel, D.; Lindahl, E. GROMACS 4: Algorithms for Highly Efficient, Load-Balanced, and Scalable Molecular Simulation. *J. Chem. Theory Comput.* **2008**, *4* (3), 435−447.
(40) Darden, T.; York, D.; Pedersen, L. Particle mesh Ewald: An N·log(N) method for Ewald sums in large systems. *J. Chem. Phys.* **1993**, *98* (12), 10089−10092.
(41) Bussi, G.; Donadio, D.; Parrinello, M. Canonical sampling through velocity rescaling. *J. Chem. Phys.* **2007**, *126* (1), No. 014101.
(42) Parrinello, M.; Rahman, A. Polymorphic transitions in single crystals: A new molecular dynamics method. *J. Appl. Phys.* **1981**, *52* (12), 7182−7190.
(43) Cook, E. C.; Featherston, E. R.; Showalter, S. A.; Cotruvo, J. A. Structural Basis for Rare Earth Element Recognition by Methylobacterium extorquens Lanmodulin. *Biochemistry* **2019**, *58* (2), 120−125.
(44) Habenschuss, A.; Spedding, F. H. The coordination (hydration) of rare earth ions in aqueous chloride solutions from x-ray diffraction. III. SmCl3, EuCl3, and series behavior. *J. Chem. Phys.* **1980**, *73* (1), 442−450.
(45) Liu, S.; Featherston, E. R.; Cotruvo, J. A.; Baiz, C. R. Lanthanide-dependent coordination interactions in lanmodulin: a 2D IR and molecular dynamics simulations study. *Phys. Chem. Chem. Phys.* **2021**, *23* (38), 21690−21700.
(46) Hoch, J. C.; Baskaran, K.; Burr, H.; Chin, J.; Eghbalnia, H. R.; Fujiwara, T.; Gryk, M. R.; Iwata, T.; Kojima, C.; Kurisu, G.; et al. Biological magnetic resonance data bank. *Nucleic Acids Res.* **2023**, *51* (D1), D368−D376.
(47) Clore, G. M. Practical Aspects of Paramagnetic Relaxation Enhancement in Biological Macromolecules. In *Methods in Enzymology*; Qin, P. Z.; Warncke, K., Eds.; Academic Press, 2015; Vol. *564*, pp 485−497.
(48) Karschin, N.; Becker, S.; Griesinger, C. Interdomain Dynamics via Paramagnetic NMR on the Highly Flexible Complex Calmodulin/Munc13−1. *J. Am. Chem. Soc.* **2022**, *144* (37), 17041−17053.
(49) Müntener, T.; Joss, D.; Häussinger, D.; Hiller, S. Pseudocontact shifts in biomolecular NMR spectroscopy. *Chem. Rev.* **2022**, *122* (10), 9422−9467.
(50) Bahramzadeh, A.; Huber, T.; Otting, G. Three-Dimensional Protein Structure Determination Using Pseudocontact Shifts of Backbone Amide Protons Generated by Double-Histidine Co2+-Binding Motifs at Multiple Sites. *Biochemistry* **2019**, *58* (30), 3243−3250.
(51) Lopez, M. M.; Chin, D. H.; Baldwin, R. L.; Makhatadze, G. I. The enthalpy of the alanine peptide helix measured by isothermal titration calorimetry using metal-binding to induce helix formation. *Proc. Natl. Acad. Sci. U.S.A.* **2002**, *99* (3), 1298−1302.
(52) Nitz, M.; Sherawat, M.; Franz, K. J.; Peisach, E.; Allen, K. N.; Imperiali, B. Structural Origin of the High Affinity of a Chemically Evolved Lanthanide-Binding Peptide. *Angew. Chem., Int. Ed.* **2004**, *43* (28), 3682−3685.
(53) Snyder, E. E.; Buoscio, B. W.; Falke, J. J. Calcium(II) site specificity: effect of size and charge on metal ion binding to an EF-hand-like site. *Biochemistry* **1990**, *29* (16), 3937−3943.
(54) Stewart, B. W.; Capo, R. C.; Hedin, B. C.; Hedin, R. S. Rare earth element resources in coal mine drainage and treatment precipitates in the Appalachian Basin, USA. *Int. J. Coal Geol.* **2017**, *169*, 28−39.

https://doi.org/10.1021/acsami.3c17565
ACS Appl. Mater. Interfaces 2024, 16, 16912−16926

(55) Easley, A. D.; Ma, T.; Eneh, C. I.; Yun, J.; Thakur, R. M.; Lutkenhaus, J. L. A practical guide to quartz crystal microbalance with dissipation monitoring of thin polymer films. *J. Polym. Sci.* **2022**, *60* (7), 1090−1107.
(56) Zhang, Y.; Du, B.; Chen, X.; Ma, H. Convergence of Dissipation and Impedance Analysis of Quartz Crystal Microbalance Studies. *Anal. Chem.* **2009**, *81* (2), 642−648.
(57) Wu, B.; Wan, J.; Zhang, Y.; Pan, B.; Lo, I. M. C. Selective Phosphate Removal from Water and Wastewater using Sorption: Process Fundamentals and Removal Mechanisms. *Environ. Sci. Technol.* **2020**, *54* (1), 50−66.
(58) Zhao, F.; Cong, Z.; Sun, H.; Ren, D. The geochemistry of rare earth elements (REE) in acid mine drainage from the Sitai coal mine, Shanxi Province, North China. *Int. J. Coal Geol.* **2007**, *70* (1), 184−192.
(59) Kalam, S.; Abu-Khamsin, S. A.; Kamal, M. S.; Patil, S. Surfactant Adsorption Isotherms: A Review. *ACS Omega* **2021**, *6* (48), 32342−32348.
(60) Azizian, S.; Eris, S.; Wilson, L. D. Re-evaluation of the century-old Langmuir isotherm for modeling adsorption phenomena in solution. *Chem. Phys.* **2018**, *513*, 99−104.
(61) Bertelsen, E. R.; Jackson, J. A.; Shafer, J. C. A Survey of Extraction Chromatographic f-Element Separations Developed by E. P. Horwitz. *Solvent Extr. Ion Exch.* **2020**, *38* (3), 251−289.
(62) Horwitz, E. P.; McAlister, D. R.; Bond, A. H.; Barrans, R. E. Novel Extraction of Chromatographic Resins Based on Tetraalkyldiglycolamides: Characterization and Potential Applications. *Solvent Extr. Ion Exch.* **2005**, *23* (3), 319−344.
(63) Piguet, C.; Bünzli, J.-C. G. Mono- and polymetallic lanthanide-containing functional assemblies: a field between tradition and novelty. *Chem. Soc. Rev.* **1999**, *28* (6), 347−358.
(64) Roca-Sabio, A.; Mato-Iglesias, M.; Esteban-Gómez, D.; Tóth, É.; de Blas, A.; Platas-Iglesias, C.; Rodríguez-Blas, T. Macrocyclic Receptor Exhibiting Unprecedented Selectivity for Light Lanthanides. *J. Am. Chem. Soc.* **2009**, *131* (9), 3331−3341.
(65) Perera, Y. R.; Xu, J. X.; Amarasekara, D. L.; Hughes, A. C.; Abbood, I.; Fitzkee, N. C. Understanding the Adsorption of Peptides and Proteins onto PEGylated Gold Nanoparticles. *Molecules* **2021**, *26* (19), No. 5788.
(66) Kegl, T.; Košak, A.; Lobnik, A.; Novak, Z.; Kralj, A. K.; Ban, I. Adsorption of rare earth metals from wastewater by nanomaterials: A review. *J. Hazard. Mater.* **2020**, *386*, No. 121632.

https://doi.org/10.1021/acsami.3c17565
ACS Appl. Mater. Interfaces 2024, 16, 16912−16926